

3D Reconstruction & Assessment Framework based on affordable 2D Lidar

Xueyang Kang¹ Yinglong Fen¹

Abstract—Lidar is extensively used in the industry and mass market, due to its measurement accuracy and insensitivity to brightness compared to cameras. It is applied onto a broad range of applications, like geodetic engineering, self driving cars or virtual reality. But the 3D Lidar with multiple beams is very expensive, and the massive measurements data can not be fully processed timely. The purpose of this paper is to explore the possibility of using cheap 2D Lidar off-the-shelf, for 3D reconstruction with high accuracy. The 3D map quality is evaluated by our proposed metrics in this paper lastly. The 3D map is constructed in two ways, one way in which the scan is performed at known positions. The other way, in which the 2D Lidar for mapping and the localization part are placed on a trolley, then the trolley is pushed on the ground. The generated maps by these approaches are converted to octomaps before the evaluation. The similarity and difference between the two maps will be evaluated by these metrics in a normalized value ranging from 0 to 1. The established mapping system is composed of several modular components. A 3D bracket is designed for assembling the Lidar with a long range, the driver and the motor. A cover platform is designed for the imu and Lidar with a shorter range but high accuracy, which will be used to implement 2D SLAM. The software is stacked up in different packages on ROS.

I. INTRODUCTION

Lidar has been one of the most anticipated sensors in recent years. It emits light pulses in some pattern, then captures the light bouncing off the surface, finally through the time of flight to infer the distance to the object, or use trigonometry to calculate the distance.

At present, the most affordable 2D Lidar sensors on the mass market are with a single laser beam. The upper part of the device containing transmitting and receiving units is mounted onto the motor shaft, hence the upper part rotates with the motor to reach a 360 degrees field of view.

Building 3D scan based on 2D laser device requires adding external rotation axes, such as, (a) adding a fixed mechanical axis. (b) by fusing the vertically mounted Lidar with positioning information from other sensors, like imu. Each of them has its own advantages and disadvantages, it needs to be selected according to the application scenario. Another issue is how to evaluate the quality of the map. Since it is difficult to obtain ground truth in reality, therefore, the metrics are usually devised to evaluate the relative map quality among all maps. But calculating the quality of the map directly based on the 3D point cloud is very computationally expensive, the

reasonable metrics to complete the evaluation, accurately and quickly should utilize existing efficient storage structure.

The paper focuses on the two 3D reconstruction methods' implementation, the sensor fusion method along movement, and the scan at multiple static locations. The remaining part of the paper is about the octree-based metrics, the rating results of the generated maps by these metrics are given lastly.

II. RELATED WORK

Many existing methods using 2D Lidar to construct 3D map is to rotate the Lidar about another axis, which is not parallel to the rotation axis of the Lidar itself, this tilting angle can be adjusted during scanning process [1]. In this way the laser beam can scan the entire three-dimensional space. There is already some open source projects about 3D reconstruction [2] in this way. Obviously, the external rotation axis adds to the complexity of the hardware, The external rotation axes should be controlled by the high precision motor. Furthermore, it is necessary to coordinate the two rotation axes, so that the lidar can sweep over the 3D area as large as possible.

To perform the 3D mapping relying only on the 2D Lidar along movement. The sensor fusion framework should integrate the position estimation and corresponding 2D scan together. The trivial work involved in the fusion is to calibrate the different sensor outputs, and synchronize the different data streams [8]. For positioning, the additional sensor like imu is used to implement odometry. However, to get the position information, the outputs of accelerometer needs to be integrated twice, consequently the drift error will accumulate over the time. The alternative is to use camera to implement visual odometry [3], [4](VO). The accuracy of the current mainstream VO algorithms is very robust, and can run in real time. However, if the scene lighting varies too much abruptly, this method will not work. Many 2D Lidar based SLAM algorithms have good robustness, at the same time, they can work even in the bad light conditions.

We will introduce the main applied 2D SLAM algorithms in ROS community briefly. "gmapping" [5] is an improved Rao-Blackwellized algorithm based on the particle filter, depending both on the Lidar and the odometer. In "gmapping", the Lidar outputs for measurement model and the odometer outputs for motion model work iteratively and asynchronously. "HectorSLAM" [6] is based on 2D grid map, the algorithm use scan match to find the optimal transform then estimate the new position. The objective

*This work was not supported by any organization

¹All authors are Master student of Electrical and Information Engineering, Technical University of Munich, Munich D-80333, Germany alexander.kang@tum.de

for optimization is a function of the occupancy probability. Each grid cell in the 2D map is registered along with the occupancy probability. Refining the approximation model is completed through the bi-linear interpolation of the probability. Hector is only dependent on the Lidar, it can register the multiple resolution maps on demand. The newly released algorithm "cartographer" [7] can achieve a good accuracy of several meters' drift over a distance of kilometer, because the loop closure detection is added into "cartographer" to minimize the drift error, and the pruned search is introduced to speed up the match search. Some SLAM algorithms utilize the topological structure in the existing world as skeleton to optimize the map, [14]. The mathematical model behind SLAM is probability, as stated in [13], [15].

The valid evaluation method is an important issue, coming with the 3D reconstruction. Traditionally, the square errors [10] can be employed when the ground truth is available. In visual field, the IoU metric [11] calculates the common pixels in two maps. To carry out the evaluation directly on the 3D point cloud generated from Lidar, is very complicated and inefficient. The solution is to convert the point cloud to the octomap [12] via ray-casting. Octree is the back-bone structure behind the octomap, in which the endpoints are represented by the 3D voxels [16].

III. SYSTEM OVERVIEW

Two types of sensors are adopted, imu and two 2D Lidar sensors, that is Sweep Scanse and Rplidar. The whole system is composed of three parts: the localization part integrates Rplidar and 9 axes Imu; the 3D mapping part, includes Sweep Scanse, stepper motor and motor driver; the back-end part on which the fusion algorithm, the post-processing pipeline, and visualization process run. Both localization and 3D mapping kits, were mounted into the 3D printed kits to be protected.

A. Hardware

The system components and transmission protocols are presented in Fig1. The Raspberry Pi 3B is employed at front-end to collect the measurements from sensors, while the laptop serves as back-end. In fusion mode, the measurements from Sweep Scanse and Rplidar, as well as the measurements from gyroscope, accelerometer, magnetometer, are sampled by Raspberry Pi 3B, and then they are wirelessly transmitted to laptop. Whereas the scan at stationary locations only requires the measurements from Sweep Scanse. and the stepper motor will provide the second rotation axis. Particularly, the stepper motor is directly driven by the dedicated PWM signals from driver. The motor driver will convert the commands from Raspberry Pi to the control sequence of stepper motor.

The communication between Raspberry Pi and laptop is through WLAN. The measurements from imu and the controlling commands for the stepper motor are transmitted via I2C, but their transmission directions are different. The two Lidar sensors are connected to Raspberry Pi by the USB cables, without extra power required.

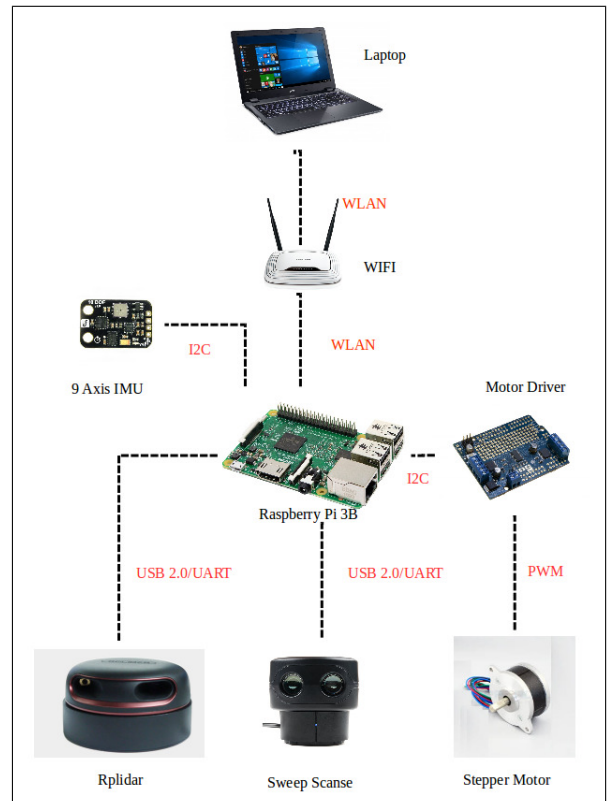


Fig. 1: System overview

The parameters provided by the Lidar suppliers are listed in the following table. Rplidar is with short range, but higher resolution, while Sweep Scanse has opposite parameters. This is mainly due to their different measurement principles, that is Rplidar uses triangulation measurement, and Sweep Scanse uses ToF. Each 2D Lidar costs 300 to 500 dollars.

TABLE I: Specifications comparison

	Sampling rate(samples/s)	Range(m)	Frequency(Hz)
Rplidar	4000	0.15-6	1-11
Sweep	1000	0.1-40	1-10

Fig. 2 shows the real measurement errors from experiments. For both Lidars, the relative error in the left y-axis drops drastically at the distance ranging from 1.5 to 2.0 meters, finally levels off at about 2%, as the measuring distance increases. But the absolute error in right y-axis initially fluctuates, then increases gradually. In general, both the relative and absolute error of Sweep Scanse are greater than those of Rplidar. It is worth noting that, the maximal range 40 meters claimed by Sweep Scanse inventor is not real. The possibility of getting valid measurements is very small at distance above 10 meters, consequently the 10 meters is adopted as a valid range at software level.

B. Software

The whole software is stacked on Ros framework hosted on *Ubuntu* system. The fusion algorithm transforms measurements from their local frames into a same global frame, and

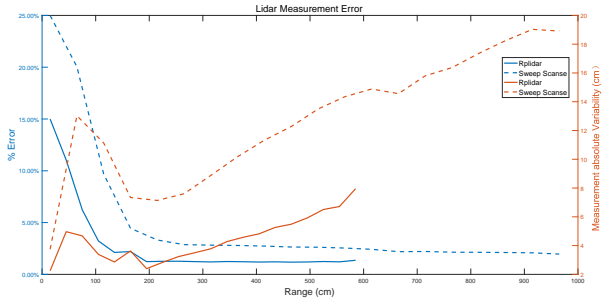


Fig. 2: Absolute and relative errors

matches the different data-streams based on their sampling time. Then the transformed point cloud is passed to the post-processing pipeline to remove outliers, and converted to octomap. Lastly, the evaluation process runs offline to compare the two maps constructed by different methods or in different hardware settings.

Fig. 3 contains all ROS nodes in the system, the arrow denotes the topic passed to the subscription node. Left block contains the driver nodes of sensors, which work on Raspberry Pi, right block contains the nodes running on laptop. Especially, the measurements from imu are processed by "Madgwick filter" [17] on Raspberry Pi, because the imu outputs are sampled at high rate, the filter implemented at front-end can avoid the transmission latency. The ROS nodes connected by the dashed arrows, are regarding the 3D reconstruction at static locations. The remaining nodes pertains to the 3D reconstruction along movement.

The "Fusion Node" fuses all the measurements from imu, Rplidar, and Sweep Scans. The pipeline from "PCL Filter Node" to "PCL to Octomap Node", all the way up to "Metric Node", is to post-process the point cloud and convert it to the octomap.

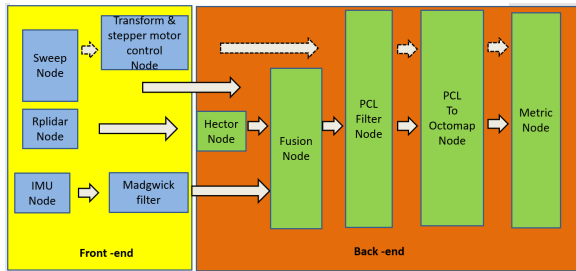


Fig. 3: Node work-flow

IV. 3D RECONSTRUCTION

3D reconstruction methods based on 2D Lidar are mainly divided into two types, as mentioned previously: 3D scan at static positions, or incremental 2D scan along movement to construct 3D point cloud.

A. 3D Reconstruction At Known Locations

The figure below shows the entire 3D scan device after installing the motor, the driver, and Raspberry Pi into the 3D printing suite.



Fig. 4: 3D scan device

The static position is provided by high precision optical instrumentation, that is (\hat{x}_p, \hat{y}_p) , the orientation ϕ of the device is defined by the stepper motor rotation angle. Each of the measurement pair, range L and bearing θ from Sweep Scans can be transformed to a point in 3D coordinate. But the bearing θ , ranging from 0° to 180° , is transformed by the current orientation ϕ , for the bearing, from 180° to 360° , the orientation ϕ of the device is at new orientation after the stepper motor's rotation at $\delta\phi$. When the beam scans to the bottom of the device, the measurement value is invalid, hence this interval can be taken advantage of, to rotate the upper part of the device.

$$\begin{aligned}
 \begin{bmatrix} x_i \\ y_i \\ z_i \end{bmatrix} &= \begin{cases} \begin{bmatrix} x_p - L \sin(\theta) \sin(\phi) \\ y_p + L \sin(\theta) \cos(\phi) \\ L \cos(\theta) \end{bmatrix} & \text{if } 0 < \theta < \pi \\ \begin{bmatrix} x_p - L \sin(\theta) \sin(\phi + \delta\phi) \\ y_p + L \sin(\theta) \cos(\phi + \delta\phi) \\ L \cos(\theta) \end{bmatrix} & \text{if } \pi < \theta < 2\pi \end{cases} \quad (1)
 \end{aligned}$$

B. 3D Reconstruction Along Movement

The incremental 2D scan along movement can build up a 3D map, here Madgwick fusion algorithm provides the heading direction based on the imu outputs. The initial position is in the same global frame as that of the 3D scan at static locations. Movement is decomposed into rotation and translation. The rotation is estimated by the two times' fusion, the first time fusion is done at front-end by Madgwick, the second time fusion is completed on laptop by Covariance Intersection, while the position is estimated only by HectorSLAM. Two-level fusion will reduce the uncertainty of the state estimation. Lastly each observation from vertical Lidar is transformed via the pose estimate after fusion at laptop.

The correlation between the two types of angle estimate sources is unknown, so we use Covariance Intersection(CI) for the secondary fusion. (μ, \hat{P}^{-1}) is the estimated angle and covariance of Madgwick, (μ', \hat{Q}^{-1}) is the estimated angle and covariance of HectorSLAM. The fused state estimate and covariance is shown below,

$$\hat{P}^{-1} = (1 - \omega)P^{-1} + \omega Q^{-1}, \omega \in (0, 1) \quad (2)$$

$$\hat{\mu} = \hat{P}((1 - \omega)\hat{P}^{-1}\mu + \omega \cdot Q^{-1}\mu')^{-1} \quad (3)$$

The Fig. 5 is the comparison chart. Integral means that using a gyroscope to directly estimate the angle, you a drift over the outputs exists. Madgwicks MSE is still relatively large, and SLAM's angle estimate is slightly better. The MSE after CI fusion is significantly reduced by half compared to that of single source.

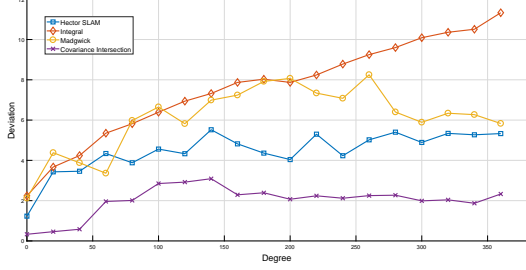


Fig. 5: Fusion accuracy comparison

All synchronization between different sensor topics is based on the time stamp at which the data is sampled. Because both Lidar sensors for mapping and localization work with low rotation frequency, so the entire trolley outfitted with all sensors in Fig. 6 was pushed along arbitrary trajectory slowly, in the experiment.



Fig. 6: Trolley outfitted with sensors

The 2D grid map with the trajectory generated by HectorSLAM is presented in figure below.

V. METRIC

In practice, 3D point cloud based evaluation is a difficult task, because its storage structure is very inefficient. Here several statistical metrics are proposed, which are implemented on octree structure. These metrics will evaluate the similarity and difference between two maps quantitatively.

A. IoU

The intersection over union is a method, applied in visual field like the work in[11], the principle is to find the common part from two compared maps, then is divided by union part from two maps. Mark "no" in the following equations indicates the unexplored areas, and the symbol "occ" is short for "occupied".

The proportions of three types of nodes in the whole octree are calculated. To count unknown nodes, a pre-defined bounding box with known length is employed, then the inner nodes with null pointers in octree are traversed by nested loops. A built-in iterator tool [12] is provided for traversing leaf nodes.

$$R_{occ} = \frac{N_{occ}}{N_{no} + N_{occ} + N_{free}} \quad (4)$$

$$R_{free} = \frac{N_{free}}{N_{no} + N_{occ} + N_{free}} \quad (5)$$

$$R_{no} = \frac{N_{no}}{N_{no} + N_{occ} + N_{free}} \quad (6)$$

Then the three IoU results corresponding to the three types of nodes are derived.

$$IoU_{occ} = \frac{Intersection_{occ}}{Union_{occ}} \quad (7)$$

$$IoU_{free} = \frac{Intersection_{free}}{Union_{free}} \quad (8)$$

$$IoU_{no} = \frac{Intersection_{no}}{Union_{no}} \quad (9)$$

Then the final weighted IoU is as Equation 10.

$$IoU = \begin{cases} R_{occ} \times IoU_{occ} + R_{free} \times IoU_{free} & \text{if } (R_{occ} + R_{free}) \leq 0.10 \\ R_{occ} \times IoU_{occ} + R_{free} \times IoU_{free} + R_{no} \times IoU_{no} & \text{if } (R_{occ} + R_{free}) > 0.10 \end{cases} \quad (10)$$

The threshold here is set according to the proportion of valid measurements in a bounding box, if the map occupies only a small fraction of the whole volume space, then the final outcome of intersection over Union should be determined only by the occupied and free sets, otherwise the measurements' difference in two maps cannot result in a remarkable difference in the overall result.

B. Log-odds

This metric is dependent only on occupied and free nodes with probability values. The metric just logs the ratio of probability values from two maps, at same spatial voxel. The log odds output of two identical maps is zero. Logarithm is applied to avoid the quotient being constant, when it near to 0 or near to 1.

$$Err = \sum_{i=1}^N \begin{cases} \log\left(\frac{p_i^{ref}}{p_i^{ar}}\right) \times p_i^{ref} & \text{if } p_i^{ref} \geq 0.9999 \\ \log\left(\frac{1-p_i^{ref}}{1-p_i^{ar}}\right) \times (1-p_i^{ref}) & \text{if } p_i^{ref} \leq 0.0001 \\ \log\left(\frac{1-p_i^{ref}}{1-p_i^{ar}}\right) \times (1-p_i^{ref}) + \log\left(\frac{p_i^{ref}}{p_i^{ar}}\right) * p_i^{ref} & \text{if } 0.0001 < p_{ref} < 0.9999 \end{cases} \quad (11)$$

The i in Equation 11 is the index for each node, N is the total number of nodes in the octree. The *ref* symbol stands for the reference, while *tar* denotes the target to be compared, The larger this metric is, the more two octomaps vary.

C. Correlation

This metric is also based on occupied and free nodes only. The coordinates of all nodes in two octrees were already transformed into a same global coordinate during 3D reconstruction process, so the evaluation of this metric can be directly implemented.

$$\rho = \frac{\sum_{x_0, y_0, z_0}^{x_N, y_N, z_N} |(p_{x_i, y_i, z_i}^{ref} - \bar{p}) \times (p_{x_i, y_i, z_i}^{tar} - \bar{p})|}{\sum_{x_0, y_0, z_0}^{x_N, y_N, z_N} (p_{x_i, y_i, z_i}^{ref} - \bar{p})^2 \times \sum_{x_0, y_0, z_0}^{x_N, y_N, z_N} (p_{x_i, y_i, z_i}^{tar} - \bar{p})^2} \quad (12)$$

In Equation 12, \bar{p} is determined by $\sum_{x_0, y_0, z_0}^{x_N, y_N, z_N} \frac{p_{x_i, y_i, z_i}^{tar} + p_{x_i, y_i, z_i}^{ref}}{2N}$, this means probability is averaged over the probabilities from intersected occupied and free nodes, x_i, y_i, z_i , states the coordinate of individual node. The larger this rating is, the more correlated the two maps are.

VI. EVALUATION RESULTS

The 3D reconstruction for a conference room is conducted in two methods, mentioned before. To verify the proposed metrics. We specially constructed three groups of 3D point clouds at static positions, in which each set of point clouds is formed by splicing several point clouds at known locations. Particularly, the lidar range was set to 10 meters and the the rotation frequency set to 1Hz, at single location, while the hardware settings of mapping Lidar, were same during the collection of other point clouds, all with 5 meters' range and 2 Hz rotation frequency.

The point clouds in the leftmost column of figures below are original. In the middle column are post-processed point clouds. Because the point clouds are with different characteristics, consequently we use different pcl filter pipelines to process them. E.g, point cloud in first row is very sparse, hence there is no need of using down-sampling.

In the following, symbol "map1" refers to point cloud 1, other and so on, especially the "ref" is used for the point clouds built-up at six locations. The Table II presents used pcl filters for individual point cloud. All point clouds go though the down-sampling and pass-through filters, but the point clouds collected from six positions is furthermore filtered by Gaussian filter to remove the outliers, because the point clouds collected at six static positions have the most points and have the highest spatial accuracy among them, hence it will be used as reference. The pass-through filter intercepts a partial point cloud from the original one, to remove the part containing the glass wall. Since the effect of glass wall on measurement is unpredictable, he comparison is only done in reliable area. The rightmost column is the octomap converted from filtered point cloud, here the octree is built up in the same voxel size.

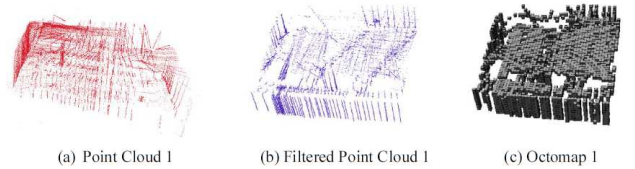


Fig. 7: Map constructed along movement

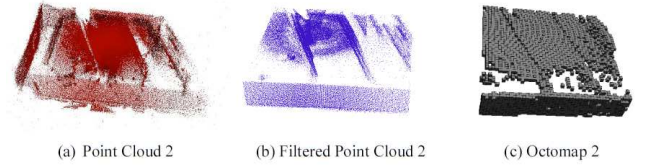


Fig. 8: Map constructed at single position

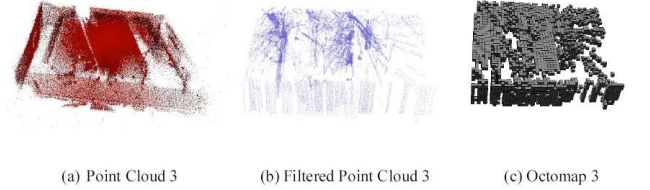


Fig. 9: Map constructed at four positions

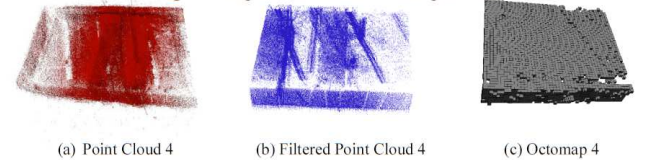


Fig. 10: Map constructed at six positions

TABLE II: Post-processing comparison

	Down-sampling)	Pass-through	Gaussian
Point Cloud 1	×	✓	×
Point Cloud 2	✓	✓	×
Point Cloud 3	✓	✓	×
Point Cloud 4	✓	✓	✓

Table II makes a basic statistical analysis over maps, unknown nodes are not taken into consideration in our case, because the point cloud filtered by pass-through filter only retains most of the valid measurement in the known area.

TABLE III: Proportion

	Occupied Ratio	Free Ratio	Leaf nodes number
map1	13.059%	86.941%	17140
map2	19.061%	80.939%	18320
map3	18.6405%	81.3595%	20553
ref	30.4077%	69.5923%	22491

Proportions of three compared octomaps are almost same, but they are different from that of reference map, so it is very hard to sort the compared octomaps by their qualities intuitively. The point cloud reconstructed incrementally along movement is very sparse, consequently its generated octomap is with many defects.

The figure below shows the final scores via different metrics above, they are all normalized. The ideal result is

at rightmost for the two same maps, log odds is zero, IoU metric and Correlation metric score one. Here the log odds is an average value over all the free and occupied nodes. The additional histogram in red is the mean probability of common nodes in the two compared octomaps, and the vertical line on top of it is the probability deviation. The final result shows that, the octomap generated from point cloud at a single location is the most consistent, then followed by the octomap from point clouds at four locations, and the octomap from point cloud reconstructed along movement is the worst.

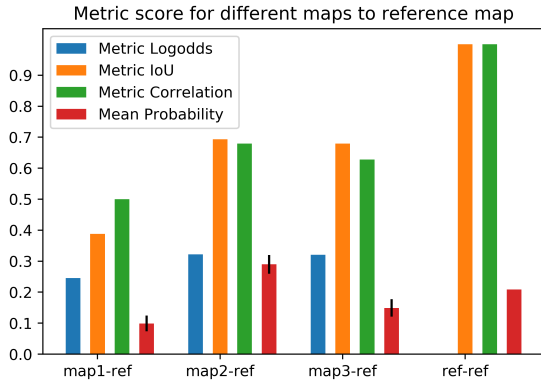


Fig. 11: Metric score

The following figure displays the required time to convert the point cloud to the octomap, and the occupied volume at different resolutions. The whole evaluation, including the all three metrics above is implemented on two exactly same octomaps at different resolutions. The smaller the size of voxel in the octree is, the smoother the reconstruction structure is. If the size is bigger than 0.25m, too many occupied cells will make the map have many enclosures, even unable to be used for navigation. However, the higher resolution increases the whole evaluation time, so a trade-off between computational time and map quality should be found. The octomap at resolution 0.20m, built-up at six positions is with 9979 nodes in the octree, the evaluation time for it takes only 75ms, therefore the metric can be implemented in real time potentially.

VII. CONCLUSIONS

Through the experimental tests, the entire system can achieve the 3D reconstruction by two means, including incremental 2D scans along movement to form the 3D point cloud, or the 3D scan completed at fixed locations, aside that, the octomap based metrics can assess the target and reference maps' similarity and difference comprehensively. The final test, also indicates that the evaluation by the proposed metrics, can be completed in a few hundred milliseconds' level, but it should be dependent on other parameters, like the total number of points and the resolution. With appropriate parameters, the metrics can be implemented while constructing the octomap incrementally, because 2D Lidar's maximal sampling rate is around 400 points per second, the

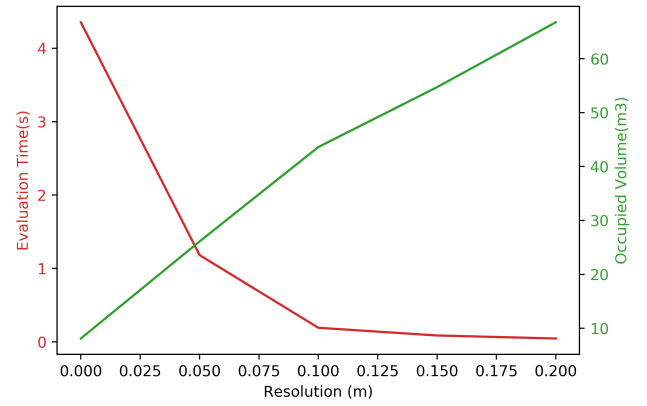


Fig. 12: Relationship between resolution and size, time

measurements in this order of magnitude, can be converted to octree nodes within a few milliseconds by ray-casting, so the total time including conversion and assessment time can be within 1 second. At the same time, we should be aware that, the use of low cost 2D lidar sensors off-the-shelf to build 3D point cloud, will either increase the complexity of the hardware, like the scan with additional controlled motor to offer another axis, or require additional sensors, which increases the complexity of the software. Because the rotation frequency of the low-cost Lidar is not high, therefore, the whole frame work are not applicable to the mapping in a fast and continuous motion. The whole 3D scan process based on 2D Lidar is also quite time-consuming. So the whole system for 3D reconstruction is only applicable to some low-speed mobile applications that are not time critical.

REFERENCES

- [1] Hu C, Huang Z, Qin S, et al. *A new 3D imaging lidar based on the high-speed 2D laser scanner*[J]. Proceedings of SPIE - The International Society for Optical Engineering, 2012, 8558(1):203-206.
- [2] Dcyong, Kent-Williams. "sweep diy 3d scanner kit" project, September 2017. <http://scanse.io/3d-scanning-kit/>.
- [3] Scaramuzza, D., Fraundorfer, F., *Visual Odometry. Part I - The First 30 Years and Fundamentals*[M]. IEEE Robotics and Automation Magazine, Volume 18, issue 4, 2011.
- [4] Fraundorfer, F., Scaramuzza, D., *Visual Odometry. Part II - Matching, Robustness, and Applications*[M], IEEE Robotics and Automation Magazine, Volume 19, issue 1, 2012.
- [5] Grisetti G, Stachniss C, Burgard W. *Improved techniques for grid mapping with rao-blackwellized particle filters*[J]. *IEEE transactions on Robotics*, 2007, 23(1): 34-46.
- [6] Kohlbrecher S, Von Stryk O, Meyer J, et al. *A flexible and scalable slam system with full 3d motion estimation*[C] *Safety, Security, and Rescue Robotics (SSRR), 2011 IEEE International Symposium on. IEEE, 2011: 155-160.*
- [7] Hess W, Kohler D, Rapp H, et al. *Real-time loop closure in 2D LIDAR SLAM*[C] *textitRobotics and Automation (ICRA), 2016 IEEE International Conference on IEEE, 2016: 1271-1278.*
- [8] Tungadi F, Kleeman L. *Time synchronization and calibration of odometry and range sensors for high-speed mobile robot mapping*[C] *Proc. Australasian Conference on Robotics and Automation. 2008.*
- [9] Schwertfeger S, Jacoff A, Scrapper C, et al. *Evaluation of maps using fixed shapes: The fiducial map metric*[C] *Proceedings of the 10th Performance Metrics for Intelligent Systems Workshop. ACM, 2010: 339-346.*

- [10] [Yairi, 2004] Yairi, T. (2004). *Covisibility-based map learning method for mobile robots*. In *PRICAI 2004: Trends in Artificial Intelligence, 8th Pacific Rim International Conference on Artificial Intelligence*, pages 703712. 46
- [11] Nowozin, Sebastian. *Optimal decisions from probabilistic models: the intersection-over-union case.*” *Proceedings of the IEEE Conference on Computer Vision and Pattern Recognition*. 2014.
- [12] Hornung A, Wurm K M, Bennewitz M, et al. *OctoMap: An efficient probabilistic 3D mapping framework based on octrees*[J]. *Autonomous Robots*, 2013, 34(3): 189-206.
- [13] By Sebastian Thrun, Wolfram Burgard and Dieter Fox. *MIT press*.
- [14] Modayil J, Beeson P, Kuipers B. *Using the topological skeleton for scalable global metrical map-building*[C] *Intelligent Robots and Systems, 2004.(IROS 2004)*. *Proceedings. 2004 IEEE/RSJ International Conference on. IEEE, 2004, 2: 1530-1536*.
- [15] Berler A, Shimony S E. *Bayes networks for sensor fusion in occupancy grids*[C] *Procs. of the Conf. on Uncertainty in Artif. Intell.* 1997.
- [16] Ryde J, Hu H. *3D mapping with multi-resolution occupied voxel lists*[J]. *Autonomous Robots*, 2010, 28(2): 169.
- [17] Tsagarakis N G, Caldwell D G, Negrello F, et al. *High Performance Humanoid Platform for Realistic Environments* [J]. *Journal of Field Robotics* 2017, 34(7): 1225-1259.